


Article

Fly Ash-Based Geopolymers as Sustainable Bifunctional Heterogeneous Catalysts and Their Reactivity in Friedel-Crafts Acylation Reactions

Mohammad I. M. Al-Zeer ^{1,2,3,*} and Kenneth J. D. MacKenzie ^{1,2} 

¹ College of Engineering and Technology, American University of the Middle East, Kuwait; kenneth.mackenzie@vuw.ac.nz

² School of Chemical and Physical Sciences, Victoria University of Wellington, Wellington 6140, New Zealand

³ MacDiarmid Institute for Advanced Materials and Nanotechnology, Victoria University of Wellington, Wellington 6140, New Zealand

* Correspondence: mohammad.al-zeer@aum.edu.kw

Received: 20 March 2019; Accepted: 17 April 2019; Published: 19 April 2019



Abstract: This study presents the synthesis, characteristics and catalytic reactivity of sustainable bifunctional heterogeneous catalysts derived from coal fly ash-based geopolymer, particularly those with a high Ca content (C-class) fly ash. The developed catalysts were synthesized at room temperature and pressure in a simple ecologically-benign procedure and their reactivity was evaluated in the Friedel-Crafts acylation of various arenes. These catalysts can be produced with multilevel porous architecture, and a combination of acidic and redox active sites allowing their use as bifunctional catalysts. The acidic sites (Lewis and Brønsted acidic sites) were generated within the catalyst framework by ion-exchange followed by thermal treatment, and redox sites that originated from the catalytically reactive fly ash components. The developed catalysts demonstrated higher reactivity than other commonly used solid catalysts such as Metal-zeolite and Metal-mesoporous silicate, heteropolyacids and zeolite imidazole frameworks (ZIF).

Keywords: fly ash-based geopolymer; heterogeneous catalysis; sustainability; redox catalysts; acylation reactions

1. Introduction

Geopolymers are an amorphous class of aluminosilicate inorganic polymers which sometimes are described as amorphous analogous of zeolites [1]. Their structure is composed of silicate and aluminate tetrahedral units randomly arranged and joined through their common oxygen atoms forming a 3D framework [2,3]. Extra-framework mono or divalent alkali cations (commonly Na⁺ or K⁺) which compensate the negative charge on the aluminate tetrahedra are capable of ion-exchange, allowing the introduction of various functionalities within the geopolymer framework [4]. Figure 1 illustrates a schematic representation of the geopolymer framework.

Due to their excellent mechanical properties, geopolymers have conventionally been used as environmentally friendly alternatives to Portland cement [5]. Geopolymers possess a number of useful features such as their porous structure, ion-exchange capability, low preparation costs, ease of synthesis and environmental friendliness. Thus, the potential of geopolymers has recently been demonstrated in various applications including drug delivery, photoluminescence, chromatography and catalysis applications [6]. In the field of heterogeneous catalysis, in particular, various catalytically active sites, acidic, basic and redox active centres, can be generated within the geopolymer framework by ion-exchange, allowing their use in a wide range of catalytic applications. Clay-based geopolymers as supports for various catalytically active transition metals and nanoparticles have recently been

reported for different applications [7–11]. More recently, clay-based geopolymers acting as true solid acid catalysts, exploiting inherent acid sites in their structure, have been developed for fine chemical applications [12,13].

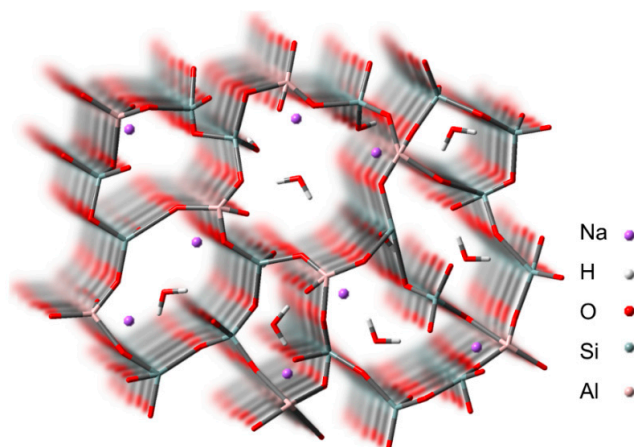
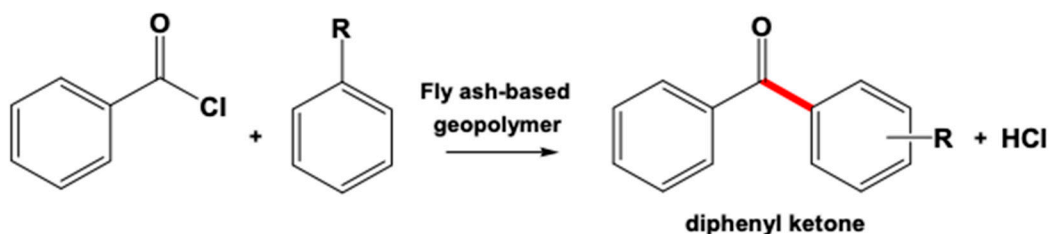


Figure 1. Schematic representation of the geopolymer framework.

Geopolymers are readily synthesised by mixing a solid aluminosilicate precursor with an alkali metal silicate under alkaline conditions, the mixture setting to a hard mass at ambient temperature in an energy-efficient and environmentally friendly process. Aluminosilicate precursors are commonly natural aluminosilicate clay or industrial wastes, such as fly ash and blast furnace slag. Using industrial wastes such as coal fly ash (the waste generated in coal-fired thermal power plants) as a precursor for geopolymer synthesis provides a useful approach to the utilisation of these abundant wastes. The major components of fly ash are SiO_2 and Al_2O_3 , but depending on the source of the coal, it may also contain a heterogeneous mixture of other catalytically active oxides such as Fe_2O_3 , TiO_2 , CaO , MgO , Na_2O , and K_2O . According to the American Society for Testing and Materials (ASTM) international C618 standard, fly ash is classified into two classes based on the CaO content; F-class fly ash contains a low Ca content (<8 wt % CaO), whereas C-class fly ash contains >8 wt % CaO . In the context of geopolymer synthesis for heterogeneous catalysis applications, the use of fly ash provides the additional advantage of the various catalytically active species present in the fly ash which contribute to the overall reactivity. Fly ash has been investigated in the field of heterogeneous catalysis either as a support for various transition metals and other active oxides [14–16], or as a precursor for catalytically-active zeolites [17,18] and mesoporous silicates [19,20]. In this process, the fly ash is the source of silica which is obtained by fusing with solid alkali at >500 °C [21,22]. The synthesis then involves crystallisation and calcination, making it time and energy consuming. On the other hand, fly ash-based geopolymers have rarely been investigated as heterogeneous catalysts. A few studies have recently reported the photocatalytic reactivities of fly ash-based geopolymers in the degradation of organic pollutants in waste water [23,24]. In addition, geopolymers derived from various fly ashes, particularly low-calcium F-class fly ash, have recently been reported to function as novel heterogeneous catalysts for industrially-important Friedel-Crafts alkylation reactions [25].

In the present paper we report the synthesis and characterisation of C-class (high-calcium) fly ash-based geopolymers as sustainable bifunctional heterogeneous catalysts and demonstrate their reactivity in the industrially demanding Friedel-Crafts acylation reactions of various arenes (Scheme 1). In geopolymer applications to date, particularly as ecologically-friendly cements for construction, most of the fly ash utilised worldwide for this purpose is F-class; C-class fly ash containing a high CaO content is usually considered less desirable for the production of geopolymer building materials since it is prone to flash setting [26]. Thus, the present work provides a useful approach to an alternative and effective use of fly ash, particularly C-class fly ash. Due to the combination of active sites within their structure, bifunctional catalysts provide the advantage of one-pot integration of several catalytic

reactions. In addition, tailoring these bifunctional sites results in enhanced catalytic reactivity if both active sites are capable of catalysing the target reaction, such as the case of Friedel-Crafts acylation reaction, for instance, which is catalysed by both acidic and redox sites. The synthesis of various bifunctional heterogeneous catalysts and their catalytic properties, particularly in biomass upgrading processes, have recently been reviewed elsewhere [27].



Scheme 1. Friedel-Crafts acylation of arenes with benzoyl chloride (BzCl) as the acylating agent.

2. Results and Discussion

2.1. Characteristics of the Materials

The geopolymers and their corresponding catalysts were analyzed by X-Ray Diffraction (XRD) (Figure 2). Since fly ash (FA) is a product of a coal combustion process, the as-received FA samples display an amorphous feature (Figure 2a) superimposed on several crystalline phases; one of these was identified as a crystalline aluminosilicate such as mullite (JCPDS file no. 15-0776) which was probably formed by a reaction of the alumina and silica during heating at very high temperature (up to 1700 °C). Other compounds present include Fe_2O_3 (JCPDS file no. 04-007-9266) and quartz (JCPDS file no. 01-070-7344).

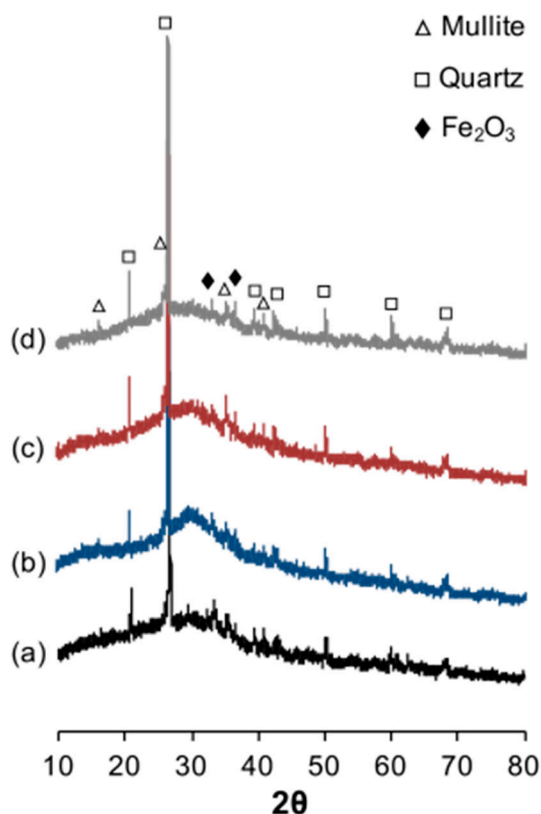


Figure 2. Representative X-Ray Diffraction (XRD) traces of Huntly fly ash (Huntly-FA) and Huntly FA-based geopolymer catalyst (Huntly-GP). (a) as-received Huntly-FA; (b) FA-based geopolymer “as-synthesised”; (c) NH_4^+ -form of the geopolymer; (d) NH_4^+ -geopolymer after heating to 550 °C.

The broad background in the range of $25\text{--}40^\circ 2\theta$ is a common fingerprint of a well-formed geopolymer (Figure 2b). Figure 2c shows increased intensity of the crystalline mullite and quartz reflections after ion-exchange with NH_4^+ ; this may be due to removal of some of the crystalline phases during the ion-exchange. The broadening of the amorphous background hump after heating the catalyst to 550°C (Figure 2d) is ascribed to the destruction of some of the crystalline phases by the thermal treatment.

Geopolymer formation was also studied by Fourier Transform Infrared Spectroscopy (FTIR). Figure 3 shows representative spectra of Huntly-FA and the corresponding Huntly-GP catalyst. The raw fly ash shows four main vibrations (Figure 3a); that octahedral Al-O and symmetric Si-O-Al stretching vibrations at $\sim 775\text{ cm}^{-1}$ and $\sim 570\text{ cm}^{-1}$ respectively [28,29]. The later may also be ascribed to Fe-O stretching vibration which usually appears in the range of $540\text{--}570\text{ cm}^{-1}$ [30]. The main peak at $\sim 1000\text{ cm}^{-1}$ and the shoulder at $\sim 1100\text{ cm}^{-1}$ are typical of solid aluminosilicates and arise from the asymmetric Si-O-Al and Si-O-Si stretching modes respectively.

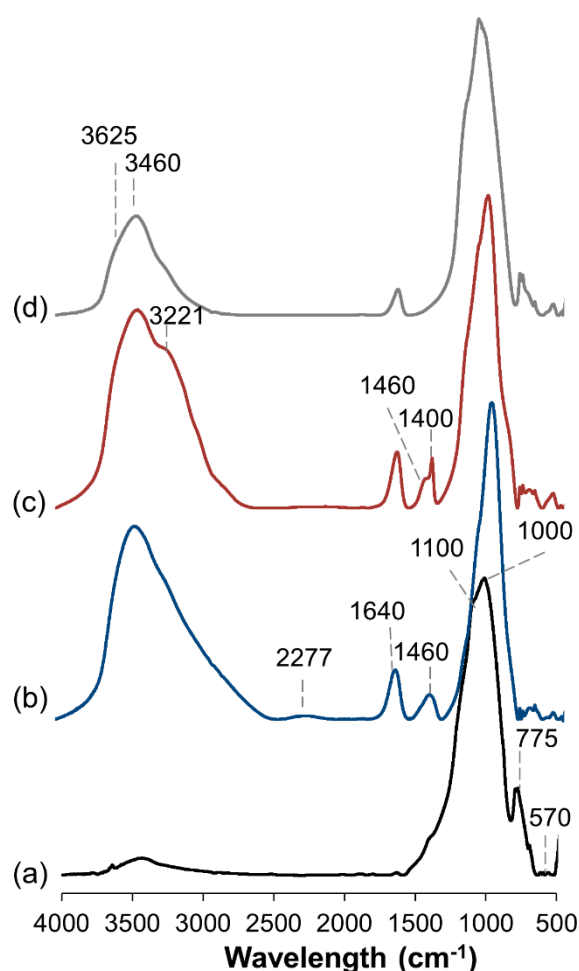


Figure 3. Representative Fourier Transform Infrared Spectroscopy (FTIR) spectra of Huntly-GP. (a) raw Huntly-FA; (b) FA-based geopolymer “as-synthesised”; (c) NH_4^+ -form of the geopolymer; (d) NH_4^+ -geopolymer after heating to 550°C .

Geopolymerisation is evidenced by the disappearance of the peak associated with the octahedral Al-O stretching mode at 775 cm^{-1} in the spectrum of the geopolymer (Figure 3b). The additional bands at ~ 1480 and 2339 cm^{-1} are associated with carbonation of the geopolymer surface by atmospheric CO_2 [31], while the peak at ~ 3500 is associated with silanol nests [32]. After NH_4^+ -ion exchange (Figure 3c), an additional peak appeared at $\sim 3200\text{ cm}^{-1}$ which is ascribed to N-H stretching mode, in addition to double peaks at ~ 1400 and 1450 cm^{-1} corresponding to N-H bending mode. The N-H

associated bands have completely disappeared after the thermal treatment at 550 °C (Figure 3d), reflecting the decomposition of NH_4^+ and thus the formation of the H-form of the geopolymer. The thermal treatment also resulted in partial destruction to the silanol groups as deduced from the intensity of the hydroxyl band ($3400\text{--}3700\text{ cm}^{-1}$). Furthermore, dealumination of the thermally treated geopolymer is evidenced by the reappearance of the peak at 775 cm^{-1} which is associated with octahedral Al (EFAI). These extra-framework Al (EFAI) commonly act as Lewis acid sites, similar to crystalline aluminosilicates (zeolites), while the bridging hydroxyls ($\sim 3625\text{ cm}^{-1}$) represent Brønsted acidic sites.

The presence of both Lewis and Brønsted acidic sites was confirmed by pyridine chemisorption (Figure 4a). The peaks at 1445 and 1600 cm^{-1} are ascribed to pyridine chemisorbed on Lewis acidic sites, and the band at $\sim 1545\text{ cm}^{-1}$ is associated with pyridine chemisorbed on Brønsted acidic sites. The small peak at 1490 cm^{-1} represents a combination of both sites [33]. Figure 4b shows the thermogravimetric analysis (TGA) profile of pyridine desorption for Huntly-GP from which the total acidity was measured (Table 1).

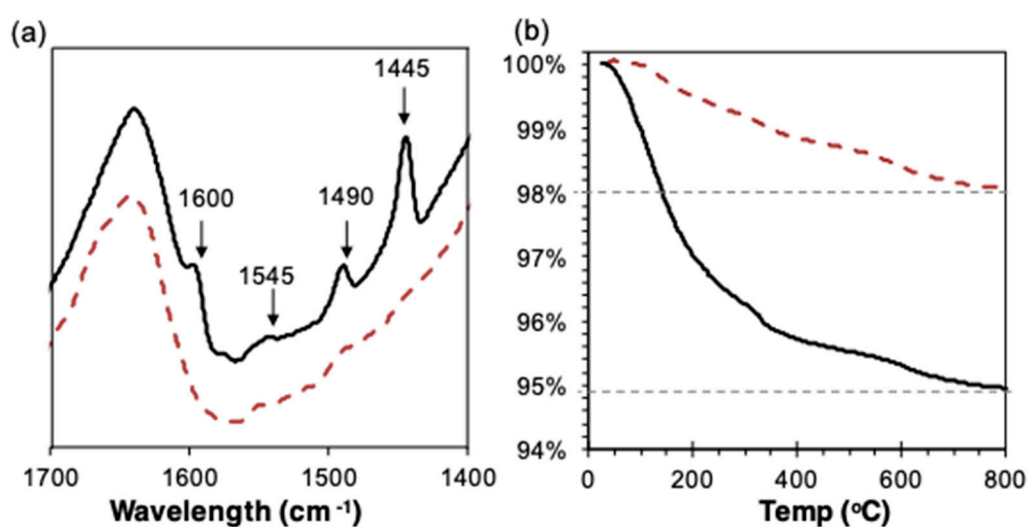


Figure 4. Acidity characterisation of Huntly-GP catalyst. (a) FTIR spectra of pyridine chemisorption; (b) thermogravimetric analysis (TGA) profile of the desorbed pyridine. The broken lines represent the background sample without pyridine.

Lewis and Brønsted acid sites are not the only active sites within the present catalysts, which also contain other catalytically active species (Table 1) such as CaO which is an active base catalyst and a promoter, and Fe_2O_3 which is an active redox catalyst for a wide range of reactions including Friedel-Crafts acylations [34]. For this reason, the distribution of these metal oxides within the formed geopolymer particles and the way they are attached to the geopolymer particles were investigated (Figure 5). High magnification scanning electron microscope (SEM) images of the Fe and Ca bright spots obtained by energy-dispersive spectrometer (EDS) show that Fe or Ca (most likely present in the geopolymer as Fe_2O_3 and CaO respectively as indicated by X-ray fluorescence (XRF) analyses) is either enclosed within the geopolymer matrix (Figure 5a) or cemented to the geopolymer particles (Figure 5b). This is advantageous over other regular supported catalysts which suffer from leaching of the active sites from the support affecting the reusability and the catalyst life time.

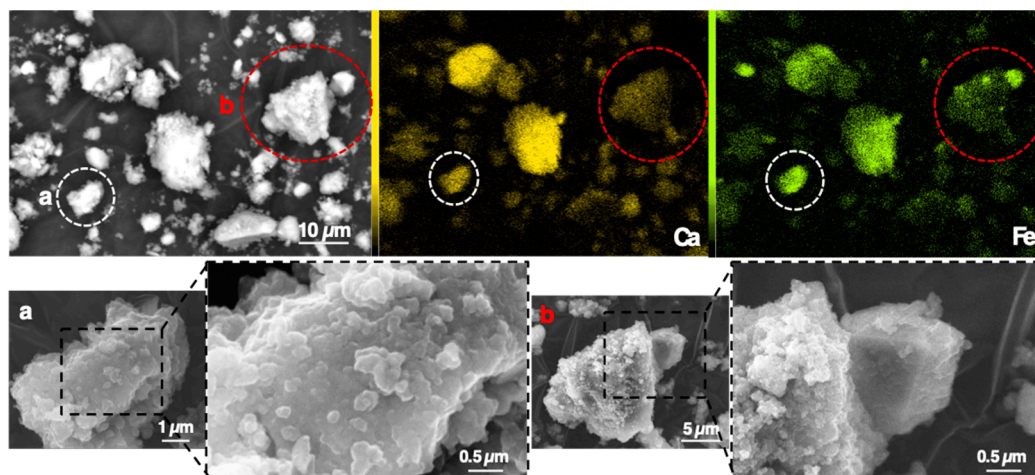


Figure 5. Backscattered scanning electron microscope (SEM) image of Huntly-GP catalyst with energy-dispersive spectrometer (EDS) maps for the Ca and Fe (top), and high magnification SEM of the circled spots (a) and (b) (bottom).

The porosity of the catalysts was investigated by N_2 sorption isotherm and transmission electron microscopy (TEM). Figure 6 shows a representative TEM image and N_2 sorption isotherm for Huntly-GP. The TEM image (Figure 6a) shows pores in the meso- ($2 \text{ nm} \leq D_{\text{pore}} \leq 50 \text{ nm}$), and macro- ($50 \text{ nm} \leq D_{\text{pore}}$) ranges. This is consistent with the N_2 sorption isotherm (Figure 6b) which shows type IV isotherms with an H3 type hysteresis loop indicative of mesoporosity; this type of hysteresis loop is associated with aggregates possessing slit-like pores [35]. However, the small pore volumes of the catalysts as suggested by the N_2 sorption isotherms (Table 1) indicates that these pores are most probably filled with amorphous debris and crystalline phases present in the original fly ash.

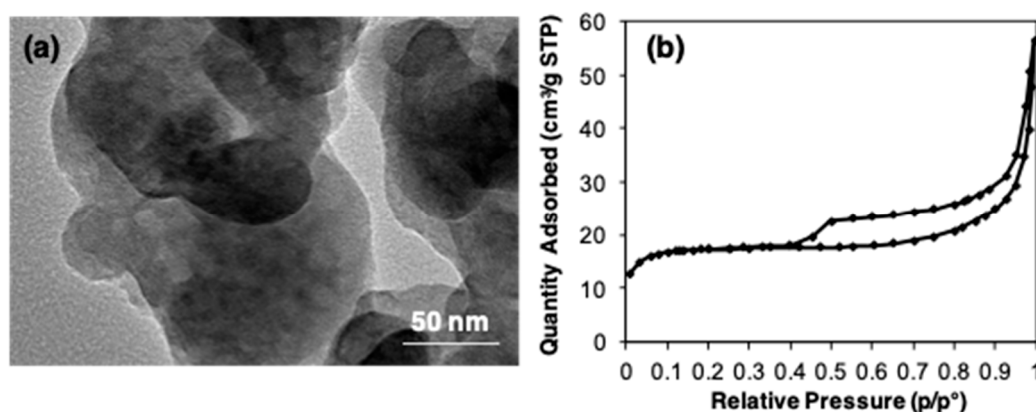


Figure 6. Porosity analysis of Huntly-GP catalyst. (a) Transmission electron microscopy (TEM) image, (b) N_2 sorption isotherm.

Table 1. Chemical and physical characteristics of the developed FA-based catalysts.

Catalyst	Acid Content (mmol/g cat.) ^a	Fe ₂ O ₃ (mmol/g cat.) ^b	CaO (mmol/g cat.) ^b	S _{BET} (m ² /g) ^c	V _{total} (cm ³ /g) ^d
Huntly-GP	0.39	0.517	1.576	59	0.09
Hyrock-GP	0.33	0.284	0.153	144	0.07

^a desorption of chemisorbed pyridine determined by TGA; ^b measured by XRF analysis; ^c measured over the range of 0.05–0.3 p/p^0 ; ^d measured as single point at $p/p^0 = 0.985$.

2.2. Catalytic Reactivity

The reactivity of the developed fly ash-based catalysts in the Friedel-Crafts acylation reactions of several substituted benzenes (toluene, anisole, *p*-xylene, and mesitylene using BzCl as the acylating agent) was first evaluated using the Huntly-GP catalyst (Figure 7 and Table 2). Figure 7 shows that the catalyst displays high catalytic reactivity in the acylation of mesitylene and anisole, giving almost complete conversion of BzCl within 2 h in the acylation of anisole, and ~95% conversion in the acylation of mesitylene. Furthermore, excellent selectivity was obtained for the acylation of both anisole and mesitylene (typically >99% towards the mono-acylated products). In the case of anisole, the main product formed was the (4-methoxyphenyl)-phenylmethanone (compound 1b, Scheme 2) with regioselectivity up to 97% and only 3% to the *ortho* isomer (compound 1a, Scheme 2). However, poor reactivity was observed in the acylation of aromatics with lower electron density on the benzene ring (e.g., the acylation of toluene and *p*-xylene with ~14 and 30% conversion of BzCl, respectively, after 3 h reaction time). This poor reactivity was also associated with low selectivity to the desired product with the principal by-product being 2-oxo-2-phenylethylformate.

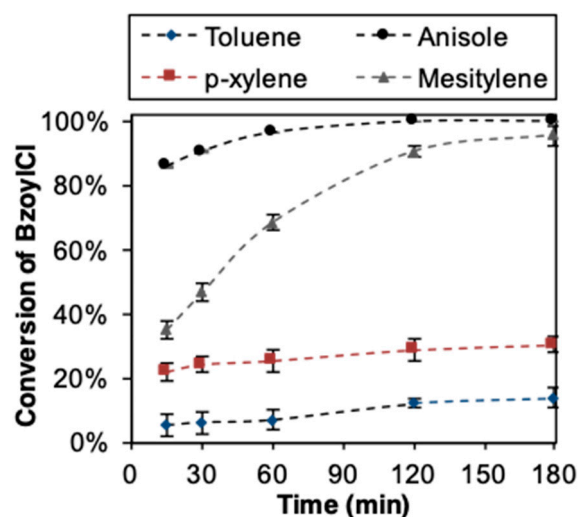
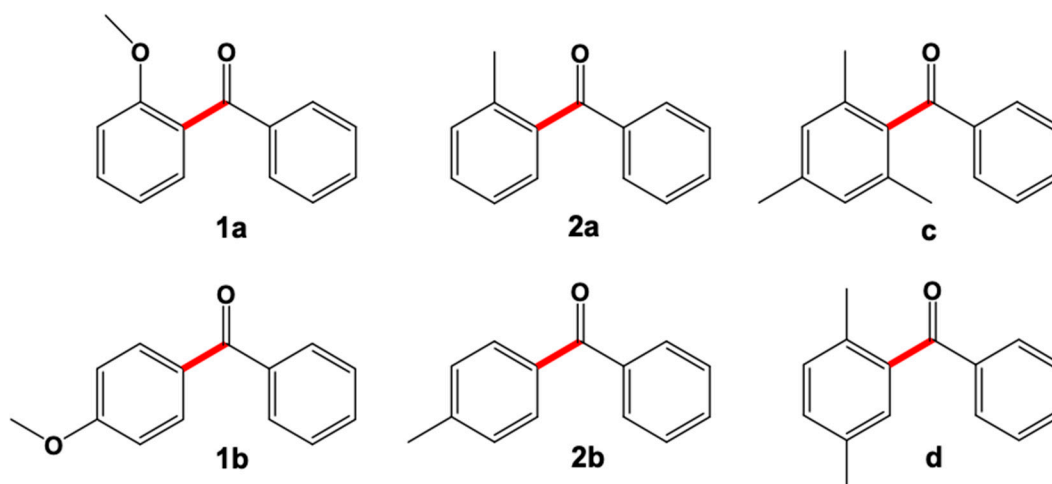


Figure 7. Reactivity of Huntly-GP catalyst in the acylation of several arenes with BzCl. Reaction conditions; 13 mL aromatic, 1 mL BzCl, 0.1 g catalyst; T = 130 °C for all aromatics except toluene 110 °C.



Scheme 2. The outcomes of the acylation reaction of different aromatics with BzCl. (1a and 1b) the monoacylated products for the acylation of anisole; (2a and 2b) the monoacylated products for the acylation of toluene; (c) and (d) the monoacylated products for the acylation of Mesitylene and *p*-xylene respectively.

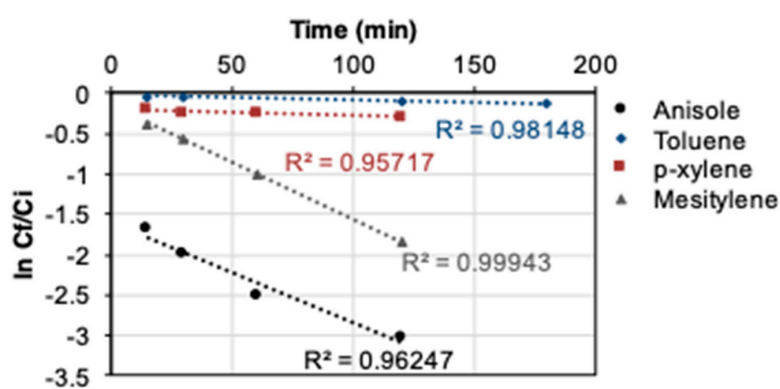
Table 2. Catalytic reactivity of Huntly-GP in the acylation of several aromatics with BzCl as the acylating agent ^a.

Substituent	Conversion (%)	Selectivity (%) [*]	Specific Reaction Rate ^b	$k (\times 10^3 \text{ min}^{-1})$	TON
Toluene ^c	14	20 (2b)	0.07	0.6	23
Anisole	100 ^d	97 (1b)	0.47	18.1	164
<i>p</i> -xylene	30	91 (d)	0.15	0.7	51
Mesitylene	96	100 (c)	0.46	14.1	159

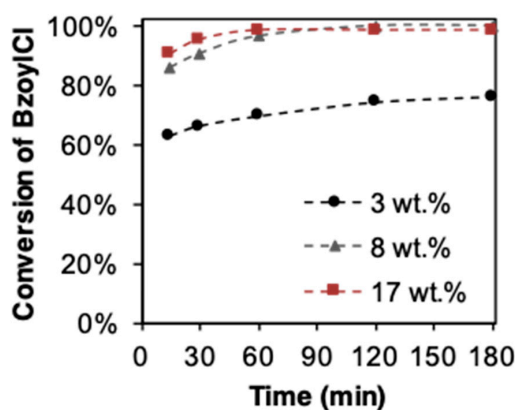
^a Reaction conditions; 13 mL aromatic, 1 mL BzCl, 0.1 g catalyst; T = 130 °C; t = 3 h; ^b ($\text{mmol}_{\text{BzCl}} \times g_{\text{cat}}^{-1} \times \text{min}^{-1}$);

^c T = 110 °C; ^d t = 2 h; ^{*} the figures in parentheses refer to compounds in Scheme 2.

These catalytic data were modelled using the Langmuir-Hinshelwood pseudo-first-order kinetic model (Figure 8), from which the reaction constants were determined (Table 2). These indicate that the reaction is most probably taking place on the surface of the catalyst rather than inside the pores, which were shown to be partially blocked by various impurities that present in the original fly ash precursor.

**Figure 8.** Langmuir-Hinshelwood pseudo-first-order kinetic model for the acylation of several aromatics over the Huntly-GP catalyst. Reaction conditions; 13 mL aromatic, 1 mL BzCl, 0.1 g catalyst; T = 130 °C for all aromatics except toluene 110 °C.

Different reactivities in the acylation of anisole were found for differing values of the catalyst: substrate wt % ratios (Figure 9). Higher reactivity was observed when more catalyst was used; a significant improvement in the catalytic reactivity was found when the catalyst: substrate wt % ratio was increased from 3 wt % to 8 and 17 wt %. This is as expected and can be ascribed to the availability of a greater number of reactive sites when more catalyst is added to the reaction mixture. Figure 9 also shows that only a slight improvement in the catalytic reactivity is obtained when the catalyst substrate wt % ratio is increased from 8 to 17 wt %, the main difference being within the first 60 min of reaction time, after which the reaction was almost complete.

**Figure 9.** Influence of the catalyst: substrate wt % on the acylation reaction of anisole with BzCl over Huntly-GP catalyst. Reaction conditions; anisole: BzCl wt % 13; T = 130 °C.

The influence of the chemical composition of the fly ash on the catalytic reactivity of the present catalyst was investigated by using a fly ash-based geopolymer synthesised from F-class Hyrock fly ash (Hyrock-GP). Table 3 shows that higher reactivity was achieved using the C-class Huntly-GP catalyst compared with the Hyrock-GP catalyst; this can be ascribed to the higher acidity and Fe₂O₃ content of the former (Table 3). However, the higher turn over number (TON) of the Hyrock-GP catalyst can be ascribed to its higher surface area (Table 1) and thus its greater available active area. This comparison reveals the viability of fly ash-based catalysts based on materials from different sources. Thus, the higher CaO content of the C-class Huntly-GP catalyst does not seem to negatively affect its catalytic performance, but in fact demonstrates higher reactivity for the acylation reactions that seem primarily to be related to the total Brønsted and Lewis acidic sites in combination with the Fe₂O₃ active sites.

Table 3. Comparison of the catalytic reactivity of various heterogeneous catalysts in Friedel-Crafts acylation of anisole.

Substituent	Conversion (%)	Selectivity (%) ^b	Specific Reaction Rate ^c	k ($\times 10^3 \text{ min}^{-1}$)	TON	TOF (min^{-1})	Ref.
Huntly-GP ^a	100	100	0.72	18.1	166 ^d	1.39	This work
Hyrock-GP ^a	92	100	0.64	6.3	270 ^d	2.25	This work
Ga/SBA-15	88	99	-	-	-	-	[36]
Fe-Na-Y	96	97	-	-	-	-	[37]
PTA-ZIF-67 ^e	82	100	-	-	-	-	[38]

^a Reaction conditions; 13 mL aromatic, 1 mL BzCl, 0.1 g catalyst; T = 130 °C; t = 120 min; ^b towards monobenzoylated product (combination of 1a and 1b, Scheme 2); ^c ($\text{mmol}_{\text{BzCl}} \times \text{g}_{\text{cat}}^{-1} \times \text{min}^{-1}$); ^d determined based on the amount of Fe₂O₃ (see Table 1); ^e phosphotungstic heteropoly acid encapsulated into zeolite imidazolate framework.

Furthermore, the catalytic performance of the Huntly-GP catalyst in the acylation of anisole and mesitylene is superior to other recently reported solid catalysts, for instance, Metal-mesoporous silicate, Fe-Na-Y zeolite, and H₃PW₁₂O₄₀ encapsulated in a ZIF-67 [38]. The present fly ash-based geopolymer catalysts provide additional advantages over these other solid catalysts since they can readily be synthesized in an energy-efficient process from industrial waste precursors, whereas other solid catalysts are costly and require sophisticated synthesis techniques.

3. Materials and Methods

3.1. Synthesis of the Parent Geopolymers

Two geopolymers were synthesized from two different fly ashes (FA); an F-class FA (Hyrock-FA) from the Bayswater power station in Australia, and a C-class FA (Huntly FA) from the Huntly power station in New Zealand. The elemental analyses of the fly ashes are shown in Table 4. The corresponding geopolymers are designated by the name of their fly ash precursor followed by GP, e.g., Huntly-GP.

The geopolymers were synthesized with the molar compositions shown in Table 5, as follows; Huntly-GP: 4 g of NaOH (Panreac, Barcelona, Spain) was dissolved in 8 mL distilled H₂O and 15 g of sodium silicate (Sod-Sil-D) (FERNZ Chemical Co., Auckland, New Zealand, Type “D”, Na₂O/SiO₂ = 0.48, solids content = 41.1 mass %) was added to the mixture. This was followed by cooling the solution to room temperature using an ice bath, then 30 g of Huntly FA was added together with 2.5 g of amorphous Al₂O₃ (Alphabond 300, Alcoa, Pittsburg, PA, USA) to adjust the SiO₂/Al₂O₃ molar ratio. Hyrock-GP was prepared by dissolving 7 g of NaOH in 17 mL distilled H₂O, cooling the solution to room temperature and adding 21 g of Hyrock FA together with 2 g Alphabond. After mixing the solution for 10 min, geopolymer resins were put in plastic molds, covered in polyethylene zipper bags and cured at 80 °C for 6 h. The molds then were uncovered and kept at 40 °C overnight. The solid geopolymer blocks were then ground to form powder with 105 µm average particle size using a vibratory mill (Bleuler; Sepor Inc., Willmington, CA, USA) fitted with a tungsten carbide pot and milling rings.

Table 4. Chemical composition of the fly ashes ^a.

Oxide (wt %)	Huntly	Hyrock
SiO ₂	46.48	66.68
Al ₂ O ₃	19.1	22.46
Na ₂ O	0.76	0.18
K ₂ O	0.69	1.05
MgO	2.85	0.56
CaO	15.56	1.09
Fe ₂ O ₃	10.2	5.79
TiO ₂	1.19	0.99
MnO	0.08	0.09
P ₂ O ₅	0.27	0.18
SO ₃	0.45	<0.01
L.O.I. ^b	1.04	0.72
Sum	98.67	99.78

^a determined by X-ray fluorescence analysis; ^b Loss on Ignition.

Table 5. Molar compositions of the fly ash-based geopolymer precursors ^a.

Molar Ratio	Hyrock-GP	Huntly-GP
SiO ₂ /Al ₂ O ₃	3.55	3.79
Na ₂ O/Al ₂ O ₃	1.34	1.10
K ₂ O/Al ₂ O ₃	0.04	0.03
H ₂ O/Al ₂ O ₃	14.32	11.23
CaO/Al ₂ O ₃	0.06	1.04
Fe ₂ O ₃ /Al ₂ O ₃	0.12	0.24
TiO ₂ /Al ₂ O ₃	0.04	0.06

^a determined by XRF.

3.2. Catalyst Preparation

The acidic forms of the two geopolymers were obtained by ion exchange to convert them to the NH₄⁺ form, followed by thermal treatment to decompose the ammonium and produce the H-form of the geopolymer. Ion-exchange of the charge-balancing alkali ions for NH₄⁺ was carried out by the method of O'Connor et al. [4]. One gram of the geopolymer powder was treated with 100 mL of 0.1 M NH₄Cl solution (Panreac) with vigorous stirring at room temperature for 12 h, washed thoroughly with a fresh solution of 0.1 M NH₄Cl, filtered, then washed again with distilled water to remove any remaining alkali ions and dried at 40 °C overnight. The ion-exchanged catalysts were then heated to 550 °C for 15 min in Carbolite electric laboratory furnace (Cole-Parmer, Vernon Hills, IL, USA) at a heating rate 15 °C/min in static air. The catalytic activities of the resulting catalysts were tested immediately after heating.

3.3. Characterisation

XRD patterns were acquired by a Bruker D8 Avance X-ray diffractometer (Billerica, MA, USA) using Cu Kα radiation operated at 45 kV and 40 mA. SEM images were obtained for carbon-coated powder using a JEOL JSM-6610 LA scanning electron microscope (Tokyo, Japan) at operating voltage of 10–20 kV, connected to an energy-dispersive spectrometer (JEOL). TEM micrographs were obtained by a JEOL JSM-2100 F transmission electron microscope at operating voltage of 200 kV. FTIR spectra were obtained by suspending the sample powder in a KBr disk and the spectra were acquired using a Perkin Elmer Spectrum One FTIR spectrometer (Waltham, MA, USA) in the range 4000–450 cm^{−1}. The acidic sites of the developed catalysts were qualitatively analysed by FTIR spectroscopy of chemisorbed pyridine, while total amount of acidic centers was determined from the desorption of pyridine using a Shimadzu TGA-50 thermal analyzer (Kyoto, Japan) following the procedure described elsewhere [13]. N₂ adsorption-desorption isotherms were determined using a Micromeritics ASAP 2010 instrument

(Norcross, GA, USA) on samples degassed at 110 °C down to 3 mTorr vacuum using the instrument degassing system. The specific surface area (S_{BET}) was measured by the Brunauer-Emmett-Teller (BET) method over a p/p^0 range of 0.05–0.3. The total pore volume (V_{total}) was measured by single point adsorption at $p/p^0 = 0.995$. The average particle size distribution was measured using a Malvern Mastersizer 2000 instrument (Norcross, GA, USA). The refractive index of the geopolymer was taken as 1.55 (similar to aluminosilicate kaolin clay).

3.4. Catalytic Reactions

The catalytic reactions in this study were performed under atmospheric pressure in a magnetic stirred 50-mL two-necked round bottom flask equipped with a reflux condenser in a thermally controlled bath. In each run, 1 mL of benzoylchloride (BzCl) was mixed with 13 mL of the aromatic compound under study (toluene, anisole, *p*-xylene or mesitylene) and the mixture was equilibrated to the reaction temperature before the addition of 0.1 g of the activated catalyst. This point was taken as the starting time of the reaction. The reaction outcomes were analyzed using GC-MS (Shimadzu QP2010-Plus).

The catalytic parameters (conversion %, selectivity %, reaction rate, turn over number (TON), and turn over frequency (TOF)) were measured as follows [39–41]:

$$\text{Conversion (\%)} = \frac{\text{amount of reactant converted (mole)}}{\text{amount of reactant fed (mole)}} \times 100\% \quad (1)$$

where the amount converted (mole) = amount fed (mole) – amount remaining (mole).

$$\text{Selectivity (\%)} = \frac{\text{amount of a particular product formed}}{\text{amount of reactant converted}} \times 100\% \quad (2)$$

$$\text{Specific rate (mol/g} \times \text{min)} = \frac{\text{amount of reactant converted (mol)}}{\text{mass of catalyst} \times \text{reaction time}} \quad (3)$$

$$\text{TON} = \frac{\text{number of moles of reactant converted per gram of catalyst}}{\text{number of moles of the active sites per gram of catalyst}} \quad (4)$$

$$\text{TOF (min}^{-1}\text{)} = \frac{\text{TON}}{\text{reaction time (min)}} \quad (5)$$

4. Conclusions

C-class coal fly ash was utilized as a precursor for a reactive, inexpensive and environmentally friendly geopolymer-based heterogeneous catalysts. The developed catalysts showed high reactivity with excellent selectivity towards the highly demanding Friedel-Crafts acylation of various arenes. The high reactivity of the geopolymer-based catalysts is ascribed to the various active sites they possess; Lewis and Brønsted acidic sites which are generated within their frameworks, and catalytically-active Fe_2O_3 species present in the original fly ash. This combination of different sites is expected to provide bifunctionality in the catalysis of acid and/or redox-catalyzed reactions. The metal oxide particles are either enclosed within the geopolymer matrix or cemented to the geopolymer particles, and thus these catalysts are expected to demonstrate a high level of reusability and catalyst life time. The catalytic performance of the geopolymer catalysts is superior to other heterogeneous catalysts whose synthesis is costly and require sophisticated procedures. In addition to their excellent catalytic reactivities, the fly ash-based geopolymer catalysts provide a valuable alternative approach to the utilization of industrial wastes such as fly ash, the vast production of which is becoming a world-wide concern.

Author Contributions: Conceptualization, M.I.M.A.-Z. and K.J.D.M.; methodology, M.I.M.A.-Z.; validation, M.I.M.A.-Z. and K.J.D.M.; formal analysis, M.I.M.A.-Z.; investigation, M.I.M.A.-Z.; resources, K.J.D.M.; data curation, M.I.M.A.-Z.; writing—original draft preparation, M.I.M.A.-Z.; writing—review and editing, K.J.D.M.; visualization, M.I.M.A.-Z.; supervision, K.J.D.M.; project administration, M.I.M.A.-Z. and K.J.D.M.

Funding: This research received no external funding.

Acknowledgments: The authors thank David Flynn for his assistance with the electron microscopy. Mohammad Alzeer is indebted to MacDiarmid Institute for Advanced Materials and Nanotechnology for the kind PhD financial support.

Conflicts of Interest: The authors declare no conflict of interest.

References

- Provis, J.L.; Lukey, G.C.; van Deventer, J.S.J. Do Geopolymers Actually Contain Nanocrystalline Zeolites? A Reexamination of Existing Results. *Chem. Mater.* **2005**, *17*, 3075–3085. [\[CrossRef\]](#)
- Duxson, P.; Fernández-Jiménez, A.; Provis, J.L.; Lukey, G.C.; Palomo, A.; van Deventer, J.S.J. Geopolymer technology: The current state of the art. *J. Mater. Sci.* **2007**, *42*, 2917–2933. [\[CrossRef\]](#)
- Yao, X.; Zhang, Z.; Zhu, H.; Chen, Y. Geopolymerization process of alkali–metakaolinite characterized by isothermal calorimetry. *Thermochim. Acta* **2009**, *493*, 49–54. [\[CrossRef\]](#)
- O'Connor, S.J.; MacKenzie, K.J.D.; Smith, M.E.; Hanna, J.V. Ion exchange in the charge-balancing sites of aluminosilicate inorganic polymers. *J. Mater. Chem.* **2010**, *20*, 10234–10240. [\[CrossRef\]](#)
- Singh, B.; Ishwarya, G.; Gupta, M.; Bhattacharyya, S.K. Geopolymer concrete: A review of some recent developments. *Constr. Build. Mater.* **2015**, *85*, 78–90. [\[CrossRef\]](#)
- MacKenzie, K.J.D. Innovative applications of inorganic polymers (geopolymers). In *Handbook of Alkali-Activated Cements, Mortars and Concretes*; Woodhead Publishing: Oxford, UK, 2015; pp. 777–805.
- Sazama, P.; Bortnovsky, O.; Dědeček, J.; Tvarůžková, Z.; Sobalík, Z. Geopolymer based catalysts—New group of catalytic materials. *Catal. Today* **2011**, *164*, 92–99. [\[CrossRef\]](#)
- Gasca-Tirado, J.R.; Manzano-Ramírez, A.; Vazquez-Landaverde, P.A.; Herrera-Díaz, E.I.; Rodríguez-Ugarte, M.E.; Rubio-Ávalos, J.C.; Amigó-Borrás, V.; Chávez-Páez, M. Ion-exchanged geopolymer for photocatalytic degradation of a volatile organic compound. *Mater. Lett.* **2014**, *134*, 222–224. [\[CrossRef\]](#)
- Gasca-Tirado, J.R.; Manzano-Ramírez, A.; Villaseñor-Mora, C.; Muñoz-Villarreal, M.S.; Zaldivar-Cadena, A.A.; Rubio-Ávalos, J.C.; Borrás, V.A.; Mendoza, R.N. Incorporation of photoactive TiO₂ in an aluminosilicate inorganic polymer by ion exchange. *Microporous Mesoporous Mater.* **2012**, *153*, 282–287. [\[CrossRef\]](#)
- Falah, M.; MacKenzie, K.J.D.; Knibbe, R.; Page, S.J.; Hanna, J.V. New composites of nanoparticle Cu (I) oxide and titania in a novel inorganic polymer (geopolymer) matrix for destruction of dyes and hazardous organic pollutants. *J. Hazard. Mater.* **2016**, *318*, 772–782. [\[CrossRef\]](#) [\[PubMed\]](#)
- Sharma, S.; Medpelli, D.; Chen, S.; Seo, D.-K. Calcium-modified hierarchically porous aluminosilicate geopolymer as a highly efficient regenerable catalyst for biodiesel production. *RSC Adv.* **2015**, *5*, 65454–65461. [\[CrossRef\]](#)
- Alzeer, M.I.M.; MacKenzie, K.J.D.; Keyzers, R.A. Facile synthesis of new hierarchical aluminosilicate inorganic polymer solid acids and their catalytic performance in alkylation reactions. *Microporous Mesoporous Mater.* **2017**, *241*, 316–325. [\[CrossRef\]](#)
- Alzeer, M.I.M.; MacKenzie, K.J.D.; Keyzers, R.A. Porous aluminosilicate inorganic polymers (geopolymers): A new class of environmentally benign heterogeneous solid acid catalysts. *Appl. Catal., A* **2016**, *524*, 173–181. [\[CrossRef\]](#)
- Wang, S.; Lu, G.Q. Effect of chemical treatment on ni/fly-ash catalysts in methane reforming with carbon dioxide. In *Studies in Surface Science and Catalysis*; Fábio Bellot Noronha, M.S., Eduardo Falabella, S.-A., Eds.; Elsevier: Amsterdam, Netherlands, 2007; Volume 167, pp. 275–280.
- Kotwal, M.S.; Niphadkar, P.S.; Deshpande, S.S.; Bokade, V.V.; Joshi, P.N. Transesterification of sunflower oil catalyzed by flyash-based solid catalysts. *Fuel* **2009**, *88*, 1773–1778. [\[CrossRef\]](#)
- Shi, Z.; Yao, S.; Sui, C. Application of fly ash supported titanium dioxide for phenol photodegradation in aqueous solution. *Catal. Sci. Tech.* **2011**, *1*, 817–822. [\[CrossRef\]](#)
- Manique, M.C.; Lacerda, L.V.; Alves, A.K.; Bergmann, C.P. Biodiesel production using coal fly ash-derived sodalite as a heterogeneous catalyst. *Fuel* **2017**, *190*, 268–273. [\[CrossRef\]](#)

18. Babajide, O.; Musyoka, N.; Petrik, L.; Ameer, F. Novel zeolite Na-X synthesized from fly ash as a heterogeneous catalyst in biodiesel production. *Catal. Today* **2012**, *190*, 54–60. [\[CrossRef\]](#)
19. Dhokte, A.O.; Khillare, S.L.; Lande, M.K.; Arbad, B.R. Synthesis, characterization of mesoporous silica materials from waste coal fly ash for the classical Mannich reaction. *J. Ind. Eng. Chem.* **2011**, *17*, 742–746. [\[CrossRef\]](#)
20. Yan, F.; Jiang, J.; Tian, S.; Liu, Z.; Shi, J.; Li, K.; Chen, X.; Xu, Y. A Green and Facile Synthesis of Ordered Mesoporous Nanosilica Using Coal Fly Ash. *ACS Sustain. Chem. Eng.* **2016**, *4*, 4654–4661. [\[CrossRef\]](#)
21. Yao, Z.T.; Xia, M.S.; Ye, Y.; Zhang, L. Synthesis of zeolite Li-ABW from fly ash by fusion method. *J. Hazard. Mater.* **2009**, *170*, 639–644. [\[CrossRef\]](#) [\[PubMed\]](#)
22. Kumar, P.; Mal, N.; Oumi, Y.; Yamana, K.; Sano, T. Mesoporous materials prepared using coal fly ash as the silicon and aluminium source. *J. Mater. Chem.* **2001**, *11*, 3285–3290. [\[CrossRef\]](#)
23. Zhang, Y.; Liu, L. Fly ash-based geopolymer as a novel photocatalyst for degradation of dye from wastewater. *Particuology* **2013**, *11*, 353–358. [\[CrossRef\]](#)
24. Strini, A.; Roviello, G.; Ricciotti, L.; Ferone, C.; Messina, F.; Schiavi, L.; Corsaro, D.; Cioffi, R. TiO₂-Based Photocatalytic Geopolymers for Nitric Oxide Degradation. *Materials* **2016**, *9*, 513. [\[CrossRef\]](#)
25. Alzeer, M.I.M.; MacKenzie, K.J.D. Synthesis and Catalytic Properties of New Sustainable Aluminosilicate Heterogeneous Catalysts Derived from Fly Ash. *ACS Sustain. Chem. Eng.* **2018**, *6*, 5273–5282. [\[CrossRef\]](#)
26. Nicholson, C.L.; Murray, B.J.; Fletcher, R.A.; Brew, D.R.M.; MacKenzie, K.J.D.; Schumucker, M. Novel geopolymer materials containing borate structural units. In *Geopolymer, Green Chemistry and Sustainable Development, Proceedings of the World Congress Geopolymer, Saint-Quentin, France, 29 June–1 July 2005*; Insitut Geopolymere: Saint-Quentin, France, 2005; pp. 31–33.
27. Sudarsanam, P.; Zhong, R.; Van den Bosch, S.; Coman, S.M.; Parvulescu, V.I.; Sels, B.F. Functionalised heterogeneous catalysts for sustainable biomass valorisation. *Chem. Soc. Rev.* **2018**, *47*, 8349–8402. [\[CrossRef\]](#)
28. Zhang, Y.; Sun, W.; Li, Z. Infrared spectroscopy study of structural nature of geopolymeric products. *J. Wuhan Univ. Technol. Mater. Sci. Ed.* **2008**, *23*, 522–527. [\[CrossRef\]](#)
29. Lee, W.K.W.; van Deventer, J.S.J. Use of Infrared Spectroscopy to Study Geopolymerization of Heterogeneous Amorphous Aluminosilicates. *Langmuir* **2003**, *19*, 8726–8734. [\[CrossRef\]](#)
30. Chen, X.; Chen, F.; Liu, F.; Yan, X.; Hu, W.; Zhang, G.; Tian, L.; Xia, Q.; Chen, X. Ag nanoparticles/hematite mesocrystals superstructure composite: a facile synthesis and enhanced heterogeneous photo-Fenton activity. *Catal. Sci. Tech.* **2016**, *6*, 4184–4191. [\[CrossRef\]](#)
31. Zukal, A.; Arian, C.O.; Delgado, M.R.; Nachtigall, P.; Pulido, A.; Mayerová, J.; Čejka, J. Combined volumetric, infrared spectroscopic and theoretical investigation of CO₂ adsorption on Na-A zeolite. *Microporous Mesoporous Mater.* **2011**, *146*, 97–105. [\[CrossRef\]](#)
32. Kim, J.; Park, W.; Ryoo, R. Surfactant-Directed Zeolite Nanosheets: A High-Performance Catalyst for Gas-Phase Beckmann Rearrangement. *ACS Catal.* **2011**, *1*, 337–341. [\[CrossRef\]](#)
33. Anilkumar, M.; Hoelderich, W.F. New non-zeolitic Nb-based catalysts for the gas-phase Beckmann rearrangement of cyclohexanone oxime to caprolactam. *J. Catal.* **2012**, *293*, 76–84. [\[CrossRef\]](#)
34. Mu, M.; Chen, L.; Liu, Y.; Fang, W.; Li, Y. An efficient Fe₂O₃/HY catalyst for Friedel-Crafts acylation of m-xylene with benzoyl chloride. *RSC Adv.* **2014**, *4*, 36951–36958. [\[CrossRef\]](#)
35. Sing, K.S. Reporting physisorption data for gas/solid systems with special reference to the determination of surface area and porosity (Recommendations 1984). *Pure Appl. Chem.* **1985**, *57*, 603–619. [\[CrossRef\]](#)
36. El Berrichi, F.Z.; Pham-Huu, C.; Cherif, L.; Louis, B.; Ledoux, M.J. Benzoylation of anisole catalyzed by Ga/SBA-15 supported on carbon nanofibers composite. *Catal. Commun.* **2011**, *12*, 790–793. [\[CrossRef\]](#)
37. Laidlaw, P.; Bethell, D.; Brown, S.M.; Hutchings, G.J. Benzoylation of substituted arenes using Zn- and Fe-exchanged zeolites as catalysts. *J. Mol. Catal. A: Chem.* **2001**, *174*, 187–191. [\[CrossRef\]](#)
38. Ammar, M.; Jiang, S.; Ji, S. Heteropoly acid encapsulated into zeolite imidazolate framework (ZIF-67) cage as an efficient heterogeneous catalyst for Friedel–Crafts acylation. *J. Solid State Chem.* **2016**, *233*, 303–310. [\[CrossRef\]](#)
39. Shi, F.; Tse, M.K.; Pohl, M.-M.; Brückner, A.; Zhang, S.; Beller, M. Tuning Catalytic Activity between Homogeneous and Heterogeneous Catalysis: Improved Activity and Selectivity of Free Nano-Fe₂O₃ in Selective Oxidations. *Angew. Chem. Int. Ed.* **2007**, *46*, 8866–8868. [\[CrossRef\]](#)

40. Lopez-Ruiz, J.A.; Davis, R.J. Decarbonylation of heptanoic acid over carbon-supported platinum nanoparticles. *Green Chem.* **2014**, *16*, 683–694. [[CrossRef](#)]
41. Haber, J. Manual on catalyst characterization (Recommendations 1991). *Pure Appl. Chem.* **1991**, *63*, 1227–1246. [[CrossRef](#)]



© 2019 by the authors. Licensee MDPI, Basel, Switzerland. This article is an open access article distributed under the terms and conditions of the Creative Commons Attribution (CC BY) license (<http://creativecommons.org/licenses/by/4.0/>).